

FAR INFRARED REFLECTANCE AND OPTICAL PROPERTIES OF
ORGANIC SUPERCONDUCTOR $(\text{TMTSF})_2\text{ClO}_4$

By

Rodica Ellison

Honours BSc, BEd, Al.I.Cuza University, Iași, Romania

A THESIS SUBMITTED IN PARTIAL FULFILLMENT OF
THE REQUIREMENTS FOR THE DEGREE OF
MASTER OF SCIENCE

in

THE FACULTY OF MATHEMATICS AND SCIENCE
DEPARTMENT OF PHYSICS

We accept this thesis as conforming
to the required standard

.....
.....
.....
.....
.....

BROCK UNIVERSITY

July, 2001

© Rodica Ellison, 2001

Acknowledgements

This is the time to acknowledge the warm welcome and the continuous support I received from the dedicated physics professors at Brock University: Dr. M. Reedyk, Dr. S. K. Bose, Dr. F. Razavi, Dr. E. Sternin, Dr. J. Black, Dr. R. Shukla, and Dr. B. Mitrović.

My work at Brock University was made possible through a research scholarship from Dr. Reedyk and the 1999 Ontario Graduate Scholarship. I am also grateful for the Physics Graduate Scholarship (donor M. Reedyk).

I thank Professor Reedyk for integrating me into the ‘experimental department’ in the H block. Her discrete presence and finely tuned guidance over the past two years have been much appreciated. Mylo Hildebrand, Aaron Slepko, and Adán Brown have been very good lab coworkers.

Dr. Reedyk helped through all the steps involved in experiment and data analysis. I acknowledge her and Dr. Mitrović’s suggestions for the final discussion of results.

Lastly, I am totally indebted to my wonderful young family (David and Alexander David), who allowed me to be a student again, in Canada. I also owe a lot to my high school and university formation, and to my family in Romania.

Abstract

Polarized reflectance measurements of the quasi 1-D charge-transfer salt $(\text{TMTSF})_2\text{ClO}_4$ were carried out using a Martin-Puplett-type polarizing interferometer and a ^3He refrigerator cryostat, at several temperatures between 0.45 K and 26 K, in the far infrared, in the 10 to 70 cm^{-1} frequency range.

Bis-tetramethyl-tetraselena-fulvalene perchlorate crystals, grown electrochemically and supplied by K. Behnia, of dimensions 2 to 4 by 0.4 by 0.2 mm, were assembled on a flat surface to form a mosaic of 1.5 by 3 mm. The needle shaped crystals were positioned parallel to each other along their long axis, which is the stacking direction of the planar TMTSF cations, exposing the *ab* plane face (parallel to which the sheets of ClO_4 anions are positioned). Reflectance measurements were performed with radiation polarized along the stacking direction in the sample.

Measurements were carried out following either a fast (15–20 K per minute) or slow (0.1 K per minute) cooling of the sample. Slow cooling permits the anions to order near 24 K, and the sample is expected to be superconducting below 1.2 K, while fast cooling yields an insulating state at low temperatures.

Upon the slow cooling the reflectance shows dependence with temperature and exhibits the 28 cm^{-1} feature reported previously [1].

Thermoreflectance for both the ‘slow’ and ‘fast’ cooling of the sample calculated relative to the 26 K reflectance data indicates that the reflectance is temperature dependent, for the slow cooling case only.

A low frequency edge in the absolute reflectance is assigned an electronic origin given

its strong temperature dependence in the relaxed state. We attribute the peak in the absolute reflectance near 30 cm^{-1} to a phonon coupled to the electronic background. Both the low frequency edge and the 30 cm^{-1} feature are noted to shift towards higher frequency, upon entering the superconducting state, by an amount of the order of the expected superconducting energy gap.

Kramers-Kronig analysis was carried out to determine the optical conductivity for the slowly cooled sample from the measured reflectance. In order to do so the low frequency data was extrapolated to zero frequency using a Hagen-Rubens behaviour, and the high frequency data was extended with the data of Cao *et al.* [2], and Kikuchi *et al.* [3]. The real part of the optical conductivity exhibits an asymmetric peak at 35 cm^{-1} , and its background at lower frequencies seems to be losing spectral weight with lowering of the temperature, leading us to presume that a narrow peak is forming at even lower frequencies.

Table of Contents

Acknowledgements	ii
Abstract	iii
1 Organic Superconductors	1
1.1 Introduction	1
1.2 $(\text{TMTSF})_2\text{X}$ Salts, Quasi One-Dimensional Systems	3
1.2.1 Crystal Structure	3
1.2.2 Electronic Structure	5
2 $(\text{TMTSF})_2\text{ClO}_4$: characterization of the compound	9
2.1 Anion Ordering and Superconducting Properties	10
2.2 Infrared Reflectance Data	13
3 Far Infrared Study of $(\text{TMTSF})_2\text{ClO}_4$	18
3.1 Introduction	18
3.2 Experimental Set-Up	19
3.3 Sample Preparation	21
3.4 Far Infrared Reflectance of $(\text{TMTSF})_2\text{ClO}_4$	23
4 Data Analysis: Thermoreflectance and Optical Conductivity	26
4.1 Thermoreflectance Below Anion-Ordering Temperature	26
4.2 Optical Conductivity	26

5	Discussion of Results and Conclusions	33
5.1	Results Discussion	33
5.2	Conclusions	37
	Appendices	39
A	Kramers-Kronig Analysis	39
	Bibliography	43

List of Figures

1.1	TMTSF molecule: chemical diagram and spatial structure. From Reference [4].	4
1.2	Crystal structure of $(\text{TMTSF})_2\text{PF}_6$, view looking down along the a -axis. From Reference [5].	5
1.3	Band structure and Fermi surface of $(\text{TMTSF})_2\text{AsF}_6$. From Reference [4].	7
2.1	Temperature dependence of resistance for nine states of $(\text{TMTSF})_2\text{ClO}_4$ given by $T_Q = 0$ K (relaxed state), 22 K, 23 K, 24 K, 24.5 K, 25 K, 26 K, 28.5 K, and 35 K. Adapted from Reference [6].	11
2.2	Phase diagram for slowly cooled $(\text{TMTSF})_2\text{ClO}_4$. From Reference [7]. . .	12
2.3	$(\text{TMTSF})_2\text{ClO}_4$ real optical conductivity along a -axis. From Cao <i>et al.</i> [2].	14
2.4	$(\text{TMTSF})_2\text{ClO}_4$ real optical conductivity at 2 K along b -axis. From Cao <i>et al.</i> [2].	16
3.1	Martin-Puplett-type polarizing interferometer, schematic overview. Adapted from Reference [8].	19
3.2	The ^3He cryostat, capable of reaching temperatures as low as 0.38 K; open overview of the sample and bolometer stages. Adapted from Reference [9].	20
3.3	$(\text{TMTSF})_2\text{ClO}_4$ reflectance along the a -axis, for the slowly cooled sample.	24
4.1	Thermoreflectance (relative to 26 K) for the slow and fast cooling of the sample, with light polarized along the a -axis.	27
4.2	Reflectance at 26 K for the slow cooling of the sample, with light polarized along the a -axis, using three different low frequency extrapolations. . . .	29

4.3	Real part of the optical conductivity for the slow cooling of the sample, at 26 K, with light polarized along the a -axis, derived from the three different low frequency extrapolations for reflectance.	30
4.4	(TMTSF) ₂ ClO ₄ real part of the optical conductivity along a -axis, for the slow cooling of the sample. Line segments indicate the magnitude of the difference due to low frequency extrapolations, at 15, 20 and 25 cm ⁻¹ . . .	31
5.1	(TMTSF) ₂ ClO ₄ reflectance, along the a -axis, for the slowly cooled sample. Notice the shift to higher frequency in the low frequency edge, on going from 1.5 K to 0.45 K.	35
5.2	The 30 cm ⁻¹ peak in reflectance along the a -axis, for the fast and the slowly cooled sample, below and above the superconducting temperature of 1.2 K.	36

Chapter 1

Organic Superconductors

1.1 Introduction

The search for a high $-T_c$ superconductor has been one of the main goals in the investigation of organic conductors. Following the Bardeen, Cooper and Schrieffer (BCS) theory of superconductivity, based on the coherent motion of paired electrons with a phonon mediated attractive interaction, W. A. Little [10] came up with the idea of extending the BCS mechanism to describe the electrons moving along an organic polymer with highly polarizable side chains.

Little's idea spurred much activity in the field of superconductor synthesis and, although such superconducting polymers have never been successfully synthesized, it had great impact on the development of the field of organic conductors. Highly conducting organic materials that have been synthesized with quasi 1-D and 2-D behaviour have brought about a new area of research at the interface of chemistry and physics.

The first organic material that proved to be superconducting under applied pressure was $(\text{TMTSF})_2\text{PF}_6$, first synthesized by Bechgaard *et al.* in 1979 [11]. By replacing PF_6 with AsF_6 , SbF_6 , ClO_4 , and ReO_4 , other organic superconductors were discovered. $(\text{TMTSF})_2\text{ClO}_4$, bis-tetramethyl-tetraselena-fulvalene perchlorate, is the only compound in this family found to date to exhibit superconductivity at ambient pressure [12].

In 1982 Parkin *et al.* [13] observed superconductivity in the sulphur-organic compound $(\text{BEDT-TTF})_4(\text{ReO}_4)_2$ (BEDT-TTF is the organic molecule bis-ethylene-di-thia

tetra-thia-fulvalene, also referred to as ‘ET’). In contrast to the TMTSF molecule, the ET molecule forms different types of compounds of varying composition ratio and crystal structure, and even different types of crystal structure for the same composition ratio. Among them a certain crystal called β -(ET)₂I₃ exhibits superconductivity at ambient pressure. It was found that by applying moderate pressure (of the order of 1 kbar) in this salt, that T_c was raised to as high as 8 K [4]. Typical ET salts have quasi 2-D electronic states. Electrons have circular motions if a magnetic field is applied perpendicular to the two dimensional conducting plane. Through the dynamics of electrons under the influence of a magnetic field, the Fermi surface and relevant physical parameters can be elucidated for the ET salts.

Since 1981 hundreds of organic conductors have been synthesized, over 50 of which are superconducting. Their superconducting temperatures have values ranging from 1.2 K to 12.6 K [14].

The discovery of the high- T_c superconductors by Bednorz and Müller in 1986 brought out the question of finding a relationship between these materials and the previously known unconventional ones, *i.e.* the organic and heavy-fermion superconductors. Other novel types have been discovered in the mean time as well, such as the alkali fullerenes [15] and the borocarbides [16].

The organic superconductors have been labeled ‘exotic’, along with the high- T_c superconductors and the heavy-fermion superconductors. Their pairing mechanisms, which may be different from the BSC one [17], remain undeciphered.

As discussed above, organic superconductors can be placed in two main families: the quasi 1-D charge transfer salts, based on the TMTSF molecule (also called Bechgaard salts), with a T_c of just over 1 K, and the quasi 2-D compounds, based on the BEDT-TTF organic molecule (also called ET salts), with a T_c of about 10 K.

From the viewpoint of materials science, of particular interest is the dependence of

observed phenomena on the molecular and crystalline structures. This can be investigated by noting the consequences of modifying the structures either chemically, by substitution of the constituent atoms or groups, or physically, by applying pressure to modify the intermolecular spacings.

This thesis concerns the experimental study of $(\text{TMTSF})_2\text{ClO}_4$, a compound from the Bechgaard salts family, $(\text{TMTSF})_2\text{X}$, in the far infrared region, by means of optical spectroscopy.

Optical spectroscopy is a well-suited technique for the study of the millimeter size, brittle $(\text{TMTSF})_2\text{ClO}_4$ crystals. This technique is not surface sensitive, since electromagnetic radiation penetrates hundreds of nanometers into the crystal. Relatively small lateral sample dimensions (0.5 mm) are enough to yield high quality spectra in the 200–1000 cm^{-1} frequency region, a region relevant to the excitations in most organics.

More powerful techniques, such as angle resolved photoemission or vacuum tunneling, demand ultrahigh-vacuum cleaved virgin surfaces and as a result have been applied to only a few systems. Magnetic neutron scattering, due to the weak interaction of the neutron with matter, demands large centimeter size crystals, which are not available for most new materials [18]. Optical spectroscopy has thus become the main spectroscopic technique for the investigation of the low lying excitations of a large range of new materials.

1.2 $(\text{TMTSF})_2\text{X}$ Salts, Quasi One-Dimensional Systems

1.2.1 Crystal Structure

A typical $(\text{TMTSF})_2\text{X}$ compound has a triclinic crystal structure. The electron donor TMTSF (tetramethyl-tetraselena-fulvalene) planar organic molecules (see Figure 1.1) are stacked in columns, the layers of columns alternating with sheets of inorganic anions, X.

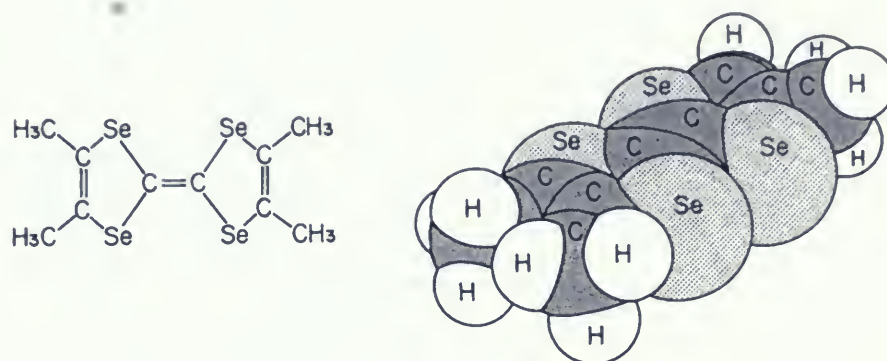


Figure 1.1: TMTSF molecule: chemical diagram and spatial structure. From Reference [4].

Figure 1.2 shows the organic cations TMTSF and inorganic anions X (PF_6 in the figure) in a plane perpendicular to the stacking direction in the crystal, *i.e.* the a -axis. The projections of the b and c axes onto this plane are denoted by b' and c' . Selenium atoms are shown as grey circles and the distances between them are given in Angströms.

The 2:1 salt is formed by the transfer of one electron from two TMTSF molecules to one X. The crystal structures are isomorphous for various electron acceptors X (PF_6 , AsF_6 , SbF_6 , with octahedral symmetry, or ClO_4 , ReO_4 , with tetrahedral symmetry), and even remain the same through substituting molecule TMTTF (tetramethyl-tetrathiafulvalene) for TMTSF (selenium atoms replaced by sulphur ones in the same configuration).

There is an electronic delocalization along the stacking direction, in the TMTSF salts, which turns these materials into a close realization of a one-dimensional metal.

In low dimensional systems the Coulomb interaction between electrons is found to have special consequences. The 'quasi-particle' concept, used in the Fermi-liquid description of ordinary metals as a collection of effectively noninteracting electrons, is not

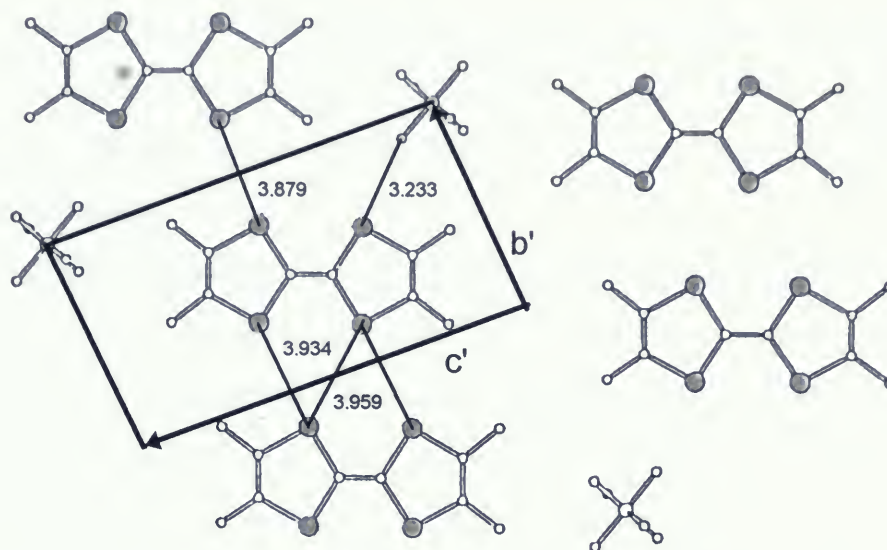


Figure 1.2: Crystal structure of (TMTSF)₂PF₆, view looking down along the *a*-axis. From Reference [5].

applicable in *one* spatial dimension, where the spin and charge degrees of freedom merge separately into collective low-energy excitations. These collective modes replace the quasi-particles, creating a different electronic state, called a ‘Luttinger liquid’ [19].

1.2.2 Electronic Structure

Along the stacking direction the spacings between the molecules are almost equal to the sum of the van-der-Waals radii of the Se atoms, approximately 3.96 Å. Although the Se–Se spacings between the side-by-side and face-by-face molecules are comparable, the overlap of the π -orbitals is strongest within the stacks, *i.e.* along the *a*-direction. There are two Se atoms on each molecule in side by side contact (in the plane of Figure 1.2) and four on each molecule in a face by face contact (along the *a*-axis, perpendicular to the plane of Figure 1.2). With this structure the intermolecular Se–Se distance, of the order of 3.8 Å, is shorter than the intrastack separation. The conductivity is highly anisotropic, the good overlap in the *a*-direction leading to a much larger transfer integral

along the a -axis of the crystal than along the b -axis. The c -direction, along which the anions and the methyl groups separate the TMTSF molecules, has the weakest coupling. The electrons move most easily along the columns but there is appreciable mobility in the b -direction as well.

In the first approximation, the counter anions X^- play no essential role in the electronic behaviour. They maintain the overall charge neutrality and separate the columns, this resulting in a low-dimensional structure. An ideal one-dimensional system cannot have long-range order and undergo a phase transition, according to the laws of thermodynamics. The TMTSF salt does have phase transitions to the superconducting and spin-density-wave (SDW) states. This can be explained by the existence of a transverse interaction (along b -axis) between adjacent TMTSF columns. It is the spacing between the sheets of columns, which depends on the size of the anions X^- , that affects the nature of the phase transition.

In the tight binding approximation, the electron band energy is expressed as:

$$E(\mathbf{k}) = 2t_a \cos(a_s k_a) + 2t_b \cos(b_s k_b) + 2t_c \cos(c_s k_c), \quad (1.1)$$

where $E(\mathbf{k})$ is the electron energy, a_s , b_s , and c_s are the intermolecular distances along the a -, b -, and c -directions, t_i is the electron transfer energy and k_i the electron wave vector along the i -direction. For simplicity the three angles have been set to 90° ; both b_s and c_s correspond to the lattice parameters b and c , while $a_s = a/2$, since a corresponds to the thickness of the TMTSF dimer.

The electron transfer energies t_a , t_b , and t_c along the a -, b -, and c -directions are estimated to be 0.25, 0.025, and 0.0015 eV, respectively, from plasma-frequency measurements and the extended Hückel calculation [20, 21]. Because the transfer energies differ greatly for the three axes, as expected from the crystal structure, the electron energy band is considered to be quasi one-dimensional in the first approximation : the

electron energy $E(\mathbf{k})$ is mostly dominated by k_a and the effects of k_b and k_c are minor. However, for phase transitions the role of k_b becomes essential. The $(\text{TMTSF})_2\text{X}$ system is thus sometimes regarded as showing a quasi two-dimensional nature.

The electron bands represented by Equation 1.1 would be filled if each TMTSF molecule were neutral. In the 2:1 charge transfer compounds $(\text{TMTSF})_2\text{X}$, since only one electron is donated from two TMTSF molecules, the band is three-fourth-filled, if the reduced Brillouin zone of the size $(2\pi)^3/a_sb_sc_s$ is used. As a result the compound is metallic. It is found that the holes in the band contribute to the conductivity, as confirmed by the observation of positive thermoelectric power [4].

In $(\text{TMTSF})_2\text{X}$ two TMTSF molecules are slid slightly towards each other, forming a sort of dimerized structure. Thus, for the electron band calculated with $a = 2a_s$ a dimerization gap opens up at $k_a = \pi/2a_s = \pi/a$. In this case the Fermi level is situated at the half filled level of the upper part of the split band.

The band structure and the Fermi surface in the first Brillouin zone of $(\text{TMTSF})_2\text{AsF}_6$ are shown in Figure 1.3. They are representative for all $(\text{TMTSF})_2\text{X}$, since the shape of

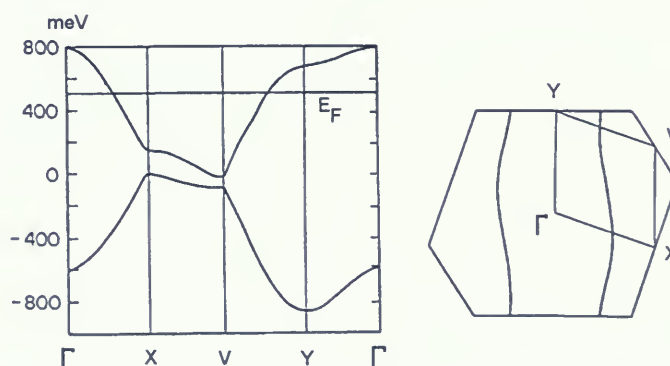


Figure 1.3: Band structure and Fermi surface of $(\text{TMTSF})_2\text{AsF}_6$. From Reference [4].

the Fermi contour is almost undistinguishable for different X.

The electronic band is based on the overlap of the π -orbitals between TMTSF molecules. The spatial distribution of the dominant π -orbitals needed here has been evaluated by

means of both ESR (electron spin resonance) and high-resolution NMR (nuclear magnetic resonance) measurements [22, 23].

Chapter 2

$(\text{TMTSF})_2\text{ClO}_4$: characterization of the compound

There is still much to be uncovered about the organic conductors' electronic properties, due mainly to the small size and fragility of the available crystals. While there is a considerable amount of infrared spectroscopy data, the strong mid-infrared absorption seen in the organics by all investigators is in clear contradiction with the extensive low temperature magnetic transport data [18]. The contradictions in the interpretation of the experiments have lead to two completely opposing views of the normal state transport of the Bechgaard salts.

In general, interpretation of the magnetic transport measurements has been done in terms of Fermi liquid models with extraordinarily long scattering times. In this framework it was found that Kohler's rule (KR) holds [24], except for the conductivity component along the a -axis. (KR states that the increase in resistivity in a magnetic field H , relative to the zero-field value ρ_0 , is a universal function of H/ρ_0 , at all temperatures T and fields H). The various oscillatory phenomena seen in high magnetic fields have been interpreted in terms of electrons moving in quasi 2-D orbits. This interpretation of the data has been summarized by Greene and Chaikin [25]. The transition to the superconducting state from a normal metallic state is also suggested by specific heat data [26].

A diametrically opposing view of the transport properties comes from the infrared research community. The low temperature measurements of the frequency dependent conductivity show that the dc-conductivity retains its large value (around $20,000 \Omega^{-1}\text{cm}^{-1}$) well into the microwave region [27, 28], but then drops dramatically in the 300 GHz region

to a value of $1000 \text{ } \Omega^{-1}\text{cm}^{-1}$ [29]. The reflectance of such a system is expected to show a prominent plasma edge in the above mentioned region, a difficult experimental range to work in with needle-like samples. There is some experimental evidence for the existence of this edge in early (1974) far infrared work by Tanner's group [29], and in more recent (1996) backward wave oscillator data from Grüner's group [28]. A clear observation of this edge would confirm the picture of two-component conductivity: a narrow Drude peak, presumably caused by a spin density wave, followed by a very broad incoherent band due to a strongly correlated Luttinger liquid [18].

2.1 Anion Ordering and Superconducting Properties

In contrast to the compounds with anions of octahedral symmetry, $(\text{TMTSF})_2\text{ClO}_4$ has intermediate and quenched states, determined by the uniformity of the orientation of the ClO_4 anions. These anions of non-centrosymmetric tetrahedral symmetry can take two orientations with respect to the crystalline system. At room temperature they are situated in a cage created by the surrounding TMTSF molecules and on cooling undergo an ordering transition. Diffuse X-ray scattering studies reveal that the anion-ordering occurs, at a temperature T_{AO} of about 24 K, to form a superlattice with the wave number $Q = (0, \frac{1}{2}, 0)$ [30]. However, when the crystal is rapidly cooled from a higher temperature to about 15 K, the anion orientations are frozen in random directions. In the slowly cooled (at a rate of 0.1 K per minute) case, at 24 K the conductivity increases with the onset of anion ordering. This is due to the reduction of scattering by the randomly distributed anion potential. With further cooling of the crystal, superconductivity appears at $T_c = 1.2$ K. By rapid cooling (30–50 K per minute), the distorted state existing above T_{AO} is quenched near 24 K and the temperature dependence of the resistivity becomes more gradual than in the case of slow cooling. An insulating phase appears

below 6 K. A mixture of these behaviours is observed when cooling conditions are intermediate and the transitions between phases become less sharp [6]. Figure 2.1 shows nine different resistance *vs.* temperature curves, taken upon slow warming of $(\text{TMTSF})_2\text{ClO}_4$ in states with various degrees of anion disorder. These intermediate states with only a

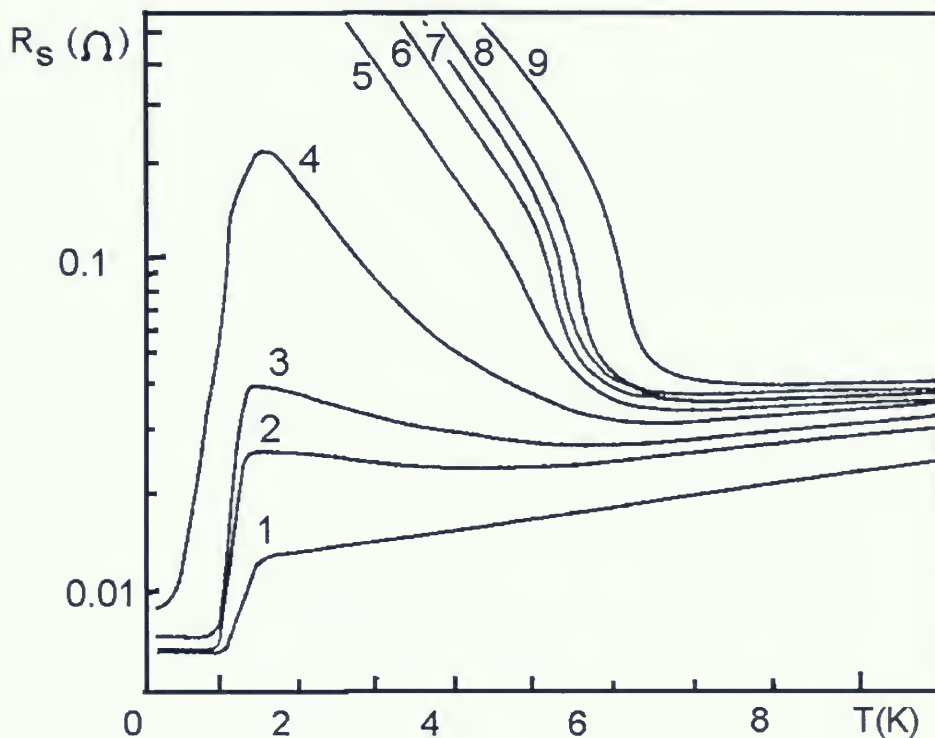


Figure 2.1: Temperature dependence of resistance for nine states of $(\text{TMTSF})_2\text{ClO}_4$ given by $T_Q = 0$ K (relaxed state), 22 K, 23 K, 24 K, 24.5 K, 25 K, 26 K, 28.5 K, and 35 K. Adapted from Reference [6].

partial degree of anion ordering were obtained by quenching (rapid cooling) the sample from various temperatures T_Q , above 24 K. The intermediate states, as characterized by resistance and magnetoresistance measurements, consist of inhomogeneous mixtures

of superconducting and spin-density-wave (SDW) regions, whereas the quenched state is purely insulating with a phase transition temperature, T_{SDW} , of 6.05 K, and a zero-temperature gap $2\Delta(0) = 22 \text{ K} = 3.52 T_{SDW}$, close to the mean field value [6].

Figure 2.2 shows the phase diagram for slowly cooled $(\text{TMTSF})_2\text{ClO}_4$, from Reference [7]. It is an extremely rich magnetic phase diagram containing metallic, supercon-

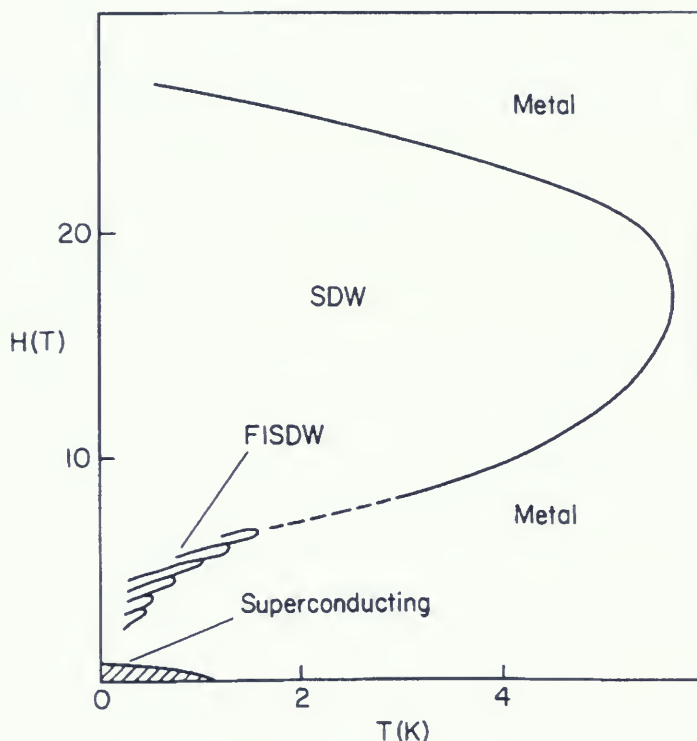


Figure 2.2: Phase diagram for slowly cooled $(\text{TMTSF})_2\text{ClO}_4$. From Reference [7].

ducting and spin-density-wave states. The magnetic field was applied in the direction of the c' -axis, along which stacks of TMTSF molecules are separated by ClO_4 anions. This is the direction in which interchain coupling is weak.

The phase diagram shows reentrance into the metallic phase with increasing field,

below 5.6 K. The critical temperature at 18 T is around 5.6 K. When the field is increased from zero, even without applying pressure, at 1 K the superconducting phase appears for H below 0.03 T. Then a normal metallic state occurs up to around 3.5 T. Between 3.5 T and 7.5 T several different SDW semimetal phases are induced by the magnetic field, as the Fermi level jumps between Landau level gaps [31]. The transitions between these field-induced spin-density-waves (FISDW) are observed, for instance, in the jumps and peaks of the specific heat which indicate first and second order transitions [32]. Between 7.5 T and 26 T a new SDW state, in which the Fermi energy changes to keep a constant Landau-level filling, appears. Above 26 T reentrance takes place into the nonmagnetic normal metal state.

2.2 Infrared Reflectance Data

The normal state far infrared optical properties of $(\text{TMTSF})_2\text{ClO}_4$ have been the object of considerable discussion over the years [33, 34, 1, 2, 35, 36].

Recent optical conductivity data with light polarized along the conducting columns (or stacks of TMTSF molecules) [2], is shown in Figure 2.3. At room temperature the graph shows a broad incoherent band (similar to that of the c -direction of the cuprates, where the carriers are confined to the planes), the low frequency limit of which tends to a value somewhat less than the dc-conductivity. As the temperature is lowered the discrepancy becomes more pronounced: the dc-conductivity is growing much faster than the real optical conductivity at measurable frequencies (the 10 K dc-conductivity is approximately $2 \times 10^5 \Omega^{-1}\text{cm}^{-1}$), which also develops a clear gap-like depression below 170 cm^{-1} (The same behaviour has been seen in the charge density wave system TTF-TCNQ [37]). Because there is a loss of spectral weight associated with the depression, it is assumed to have shifted into a low frequency mode.

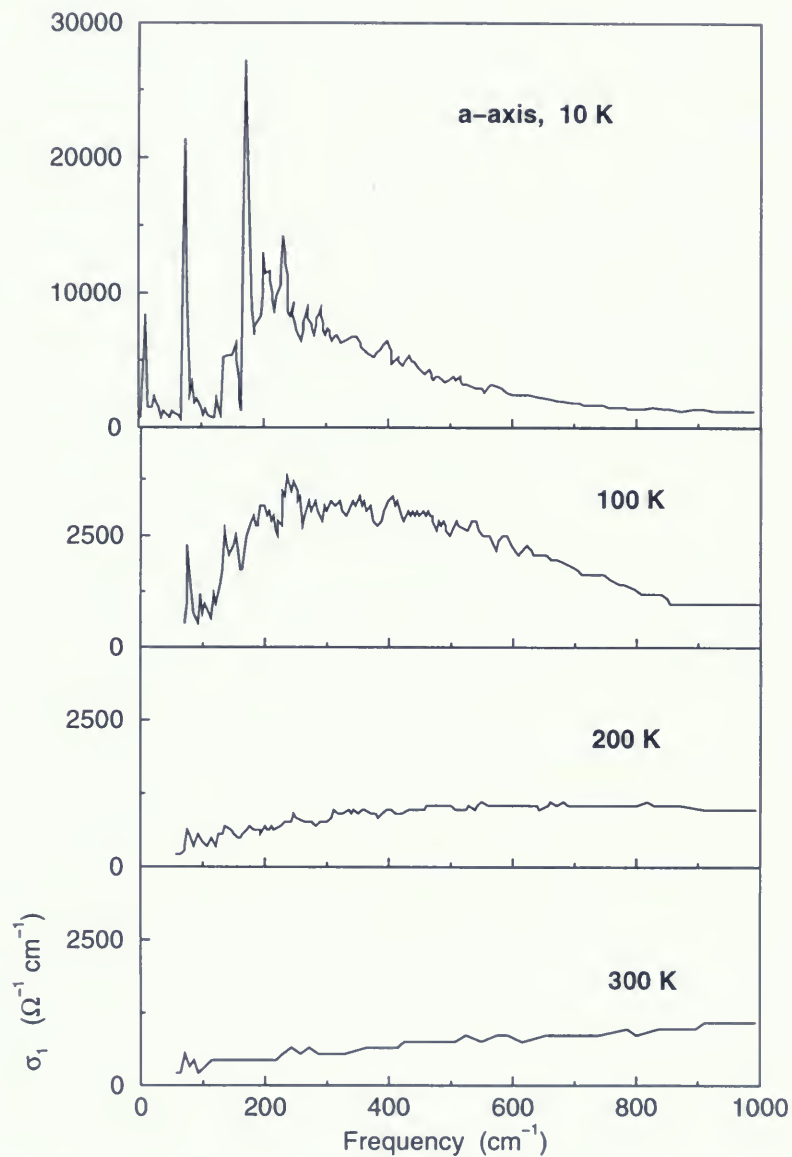


Figure 2.3: $(\text{TMTSF})_2\text{ClO}_4$ real optical conductivity along a -axis. From Cao *et al.* [2].

These data have been interpreted in terms of transport by charge-density-wave (CDW) fluctuations, according to Tanner *et al.* [29]. The observed growth in the intensity of phonon lines with lowering temperature is usually associated with sliding density waves interacting with the lattice [38, 39]. Also, estimates of the spectral weight associated with the narrow low frequency mode (the low value of which would correspond to a very large effective mass, of approximately $500 m_e$) suggest that phonons are involved as well. The high dc-conductivity is interpreted [18] to result from this far infrared narrow collective mode, associated with direct transitions across the charge density wave gap [40, 41].

The picture of transport along the stacking axis by charge density fluctuations is mainly based on the assumption that strong infrared absorption is due to intrinsic bulk effects. There are some differences in the infrared data from various laboratories, however, suggesting that sample quality may be a problem [2], which leads to the idea that surface defects, such as cracks, may be responsible for the absorption as well.

To investigate this problem, to see if the strong mid-infrared absorption is intrinsic, samples with better controlled surfaces should be used. Then, if absorption is proved to be intrinsic, reflectance measurements in high magnetic fields should be made to determine if sufficiently strong fields would break up the density wave and turn the material into a quasi 1-D metal. According to Timusk [18], this might be the case.

As can be seen in Figure 2.4, in the b -direction of $(\text{TMTSF})_2\text{ClO}_4$ (normal to the conducting stacks, between which there is still considerable overlap) the conductivity is flat, similar to the case of the c -axis cuprates [18]. There is some evidence of a collective mode, since the dc-conductivity is considerably higher (close to $1000 \Omega^{-1}\text{cm}^{-1}$) than the infrared conductivity, however, with a much smaller discrepancy than in the a -direction at low temperature. The scattering rate assigned to this flat conductivity would be of the order of 350 cm^{-1} , or 40 meV. This has to be compared with the transfer matrix element normal to the chains, t_\perp , estimated at 40 meV [18]. In terms of a Fermi liquid picture,

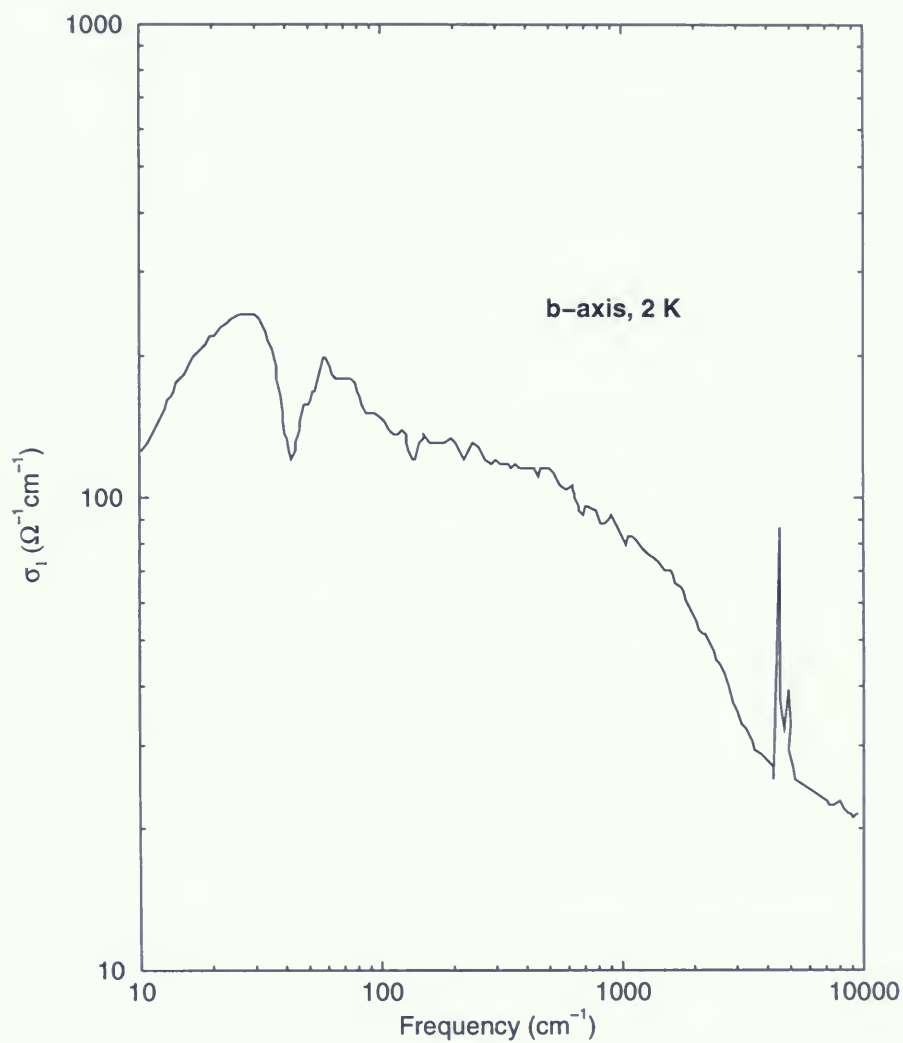


Figure 2.4: $(\text{TMTSF})_2\text{ClO}_4$ real optical conductivity at 2 K along b -axis. From Cao *et al.* [2].

it should be expected that below a crossover temperature of 460 K, corresponding to 40 meV, coherence would develop and the material would become a 2-D Fermi liquid. It is clear that the transport between the chains, down to 2 K, is completely incoherent.

The organic superconductors thus display anomalous properties in the infrared. There is no evidence of simple metallic transport in any direction: along the chains the currents are carried by collective modes, possibly sliding charge density waves, and normal to the chains there is complete incoherence, similar to what is seen in the interplane transport in the cuprates [18].

Chapter 3

Far Infrared Study of $(\text{TMTSF})_2\text{ClO}_4$

3.1 Introduction

The organic conductors' optical properties in the superconducting state have been little investigated, mainly because of the low transition temperature, T_c , and the low frequency range of the expected superconducting gap. It is hoped, if larger crystals and equipment to reach lower temperatures and frequencies become available, that the superconducting gap will be investigated, as well as the transition region between the high dc- and microwave conductivity and the strongly absorbing pseudogap range.

Kramers-Kronig analysis processes reflectance data to yield the real and imaginary parts of the optical conductivity. In systems with s-wave dirty limit superconductivity, optical methods were first used to study the energy gap, and later the spectrum of excitations. That is, infrared techniques can be used to measure the optical conductivity of quasiparticles below T_c , *i.e.* in the superconducting state, where the dc-conductivity becomes infinite and shorts out all parallel channels of superconductivity [42]. Optical spectroscopy can also be used to determine the superconducting penetration depth tensor.

The present work is aimed at studying the behaviour of $(\text{TMTSF})_2\text{ClO}_4$ in the far infrared, at temperatures below the superconducting transition, which has not been investigated before, as well as below the anion ordering temperature of 24 K. The use of a ^3He cryostat allows one to access temperatures as low as 0.38 K, with filtering and detection appropriate for far infrared polarized radiation.

3.2 Experimental Set-Up

A Martin-Puplett-type polarizing interferometer is used to produce an interferogram, which is Fourier transformed to produce a spectrum of intensity as a function of frequency. A broad band source of linearly polarized light composed of all frequencies is incident upon the sample so that information is gathered from all frequencies simultaneously.

As shown in Figure 3.1, inside the interferometer the light from the mercury-xenon lamp (L) falls onto mirrors M_1 , M_2 , and M_3 , then through a polarizing grid (P), and

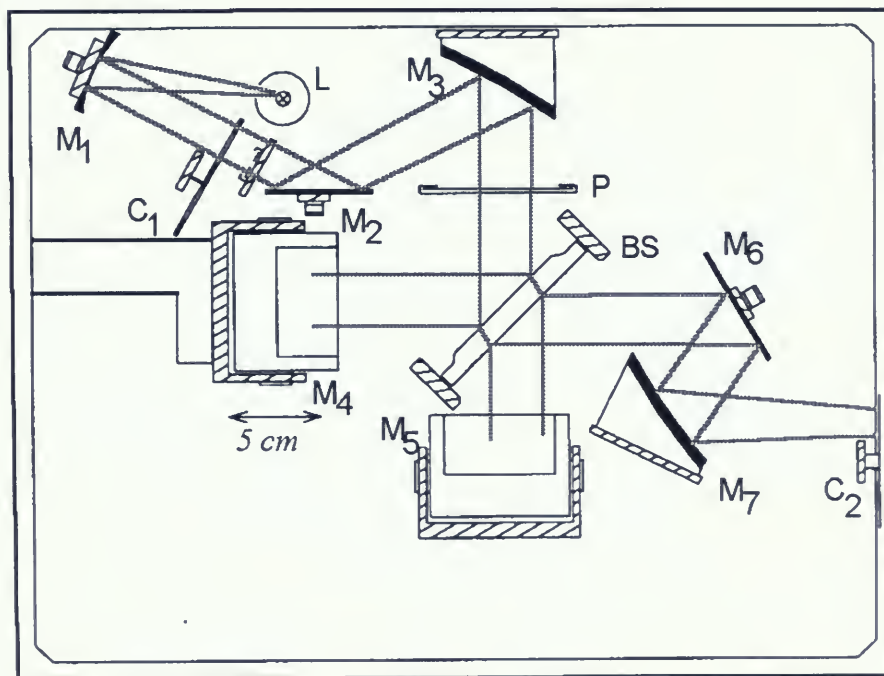


Figure 3.1: Martin-Puplett-type polarizing interferometer, schematic overview. Adapted from Reference [8].

then is separated into two beams by a polarizing beamsplitter (BS). Each beam reflects onto a 90-degree-roof-shaped mirror which rotates the polarization direction by 90° (M_4 –

moving mirror, M_5 – fixed mirror). Recombination of the two beams takes place back at the beamsplitter, where interference occurs. The resulting light pattern is then directed through a polarizing chopper (C_2) towards either the sample or the reference mirror, through a set of lightpipes connecting the interferometer to the ^3He cryostat.

Inside the cryostat (Figure 3.2) the light beam is reflected, alternately, from the sample and the mirror, and then successively received by a bolometric detector. Black poly on crystalline quartz filters were used along the light path for selecting the range

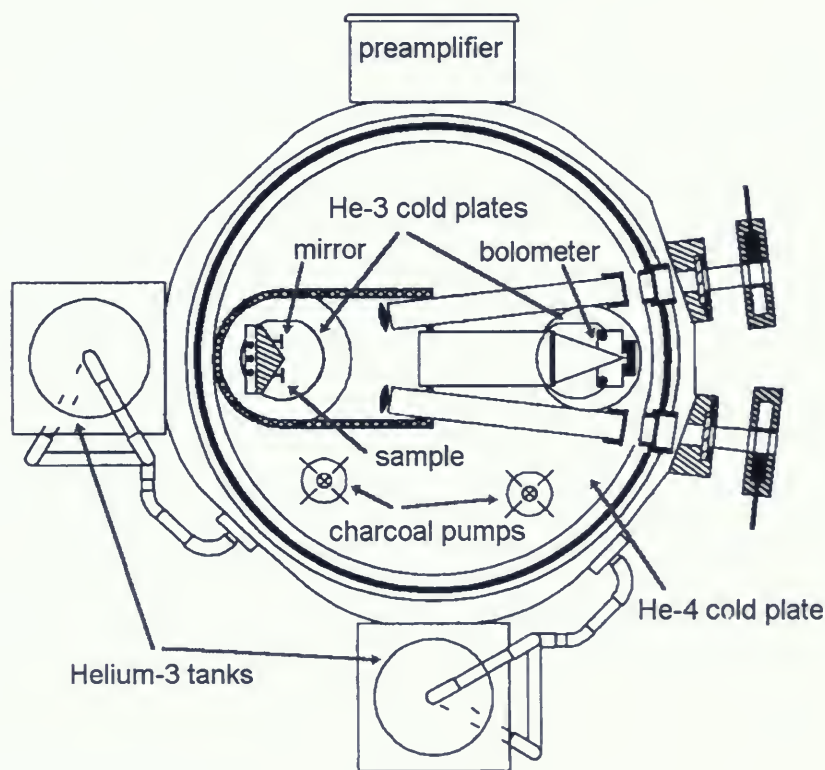


Figure 3.2: The ^3He cryostat, capable of reaching temperatures as low as 0.38 K; open overview of the sample and bolometer stages. Adapted from Reference [9].

of the spectrum of interest. The cryostat has separate stages for the sample and the

detector, which are thermally isolated from one another, thus allowing the bolometer to be maintained at the temperature for ideal detection, while the sample temperature is varied. The ^3He cryostat can reach temperatures as low as 0.38 K and allows one to obtain reliable data to as high as 90 K, at which point the two stages are no longer thermally isolated from each other. For the experiments presented here a silicon bolometer was used, optimized for performance at 0.32 K [9], and the system windows were crystalline quartz.

For reflectance measurements an accuracy of the order of less than a percent is required, since the reflectance is greater than 0.8, *i.e.* within 20% of the maximum value, 1. Due to the irregularity and discontinuity of the reflecting surface of the mosaic sample, obtaining accurate data requires the adoption of a complex normalization procedure for the reflectance data. The measured reflectance spectrum is derived as the ratio between the power reflected from the sample surface and that reflected from the sample itself coated with a thin layer of gold. To correct for instrumental fluctuations, the resulting spectrum is also multiplied by the inverse ratio of two reflectance spectra measured from a flat mirror, aligned in the same plane with the sample, before and after gold deposition.

For the gold-coating of the sample an in-situ evaporation technique is used [43], in order to keep all positional parameters and ambient conditions the same. The ratioing of the spectra before and after coating is aimed at eliminating the contribution of surface irregularities.

3.3 Sample Preparation

The sample studied was a mosaic of eight single crystals of $(\text{TMTSF})_2\text{ClO}_4$, selected from about twelve single crystals supplied by K. Behnia. The crystals were synthesized by electrocrystallization (usually on a platinum anode [44]) and had a needle-like shape,

with dimensions varying from 0.2 mm to 4 mm.

For reflectance measurements only the longest crystals were chosen, to ensure that they could be aligned parallel with each other (*i.e.* along the a -axis), and a mosaic surface as flat and continuous as possible was obtained.

A plane surface was prepared on a copper post which had been heat treated and cleaned by immersion in sulfuric acid solution. With the aid of a microscope, the crystals were picked up by static adherence to the tip of a thin plastic needle. Because the crystals were very brittle and would break at the touch of a hard metal object tweezers had to be abandoned.

5-minute-epoxy was applied to the 1.5 by 3 mm copper surface, onto which the crystals were positioned parallel and close together, so that almost no glue would show through. Some crystals longer than 3 mm had to be shortened to dimension, to eliminate the risk of them breaking during the experiment. The crystals forming the mosaic were seen to be solidly glued to the surface. The copper post had already been installed on the sample holder to minimize wear due to handling of the sample, after mounting. As shown in Figure 3.2, the sample holder is a solid copper piece having two mirror like surfaces with a 98° angle between them, designed to direct light which misses the sample or reference mirror to the walls of the housing chamber, which are coated with absorbing foam. The sample and reference mirror are mounted, one on each side, on protruding copper posts screwed into the flats at such an angle as to direct incident light to the detector.

With an in-situ evaporation technique the sample was coated with gold for the second part of the experiment. Measurements were done with light polarized along the a -axis.

3.4 Far Infrared Reflectance of $(\text{TMTSF})_2\text{ClO}_4$

Reflectance was measured for $(\text{TMTSF})_2\text{ClO}_4$ along the a -axis in three sets of experiments. First the sample was cooled at a rate of approximately 15–20 K per minute through the anion-ordering temperature of 24 K, from about 40 K to 10 K, by keeping it in close contact with the ^4He cold plate while transferring the liquid helium. Cooling at this rate is referred to in the literature as ‘rapid’ or ‘fast’ cooling. Using the routine procedure [9] the temperature of the sample was further lowered to 0.38 K. Data sets were collected at temperatures of 0.45 K, 6 K, 16 K, and 26 K, upon warming.

For the next set of experiments the sample was cooled again from 90 K, this time slowly enough (approximately 0.1 K per minute) so that the anion ordering would take place, at about 24 K, and thus the superconducting phase would appear, under 1.2 K. The rate of cooling was controlled by very slowly adjusting the thermal contact of the sample stage with the ^4He cold plate. Data sets were collected upon warming for 0.45 K, 1.5 K, 12 K, and 26 K.

Lastly, to determine the absolute value of the reflectance, as mentioned before, gold was evaporated in-situ on the reflecting surface of the sample and more data sets taken of the gold surface reflectance (which was found to be independent of the cooling rate, as expected).

About eight consistent data sets, obtained by dividing reflectance of the sample by reflectance of the reference mirror, were averaged for each temperature and then the result divided by the gold-coated-sample average spectrum.

Far infrared reflectance measured for light polarized parallel to the a -axis of the sample is shown in Figure 3.3, for the sample cooled through the anion ordering temperature of 24 K at a rate of 0.1 K per minute. This rate of cooling is referred to as ‘slow’ cooling. Temperatures include one above but close to, (1.5 K), and below, (0.45 K), the

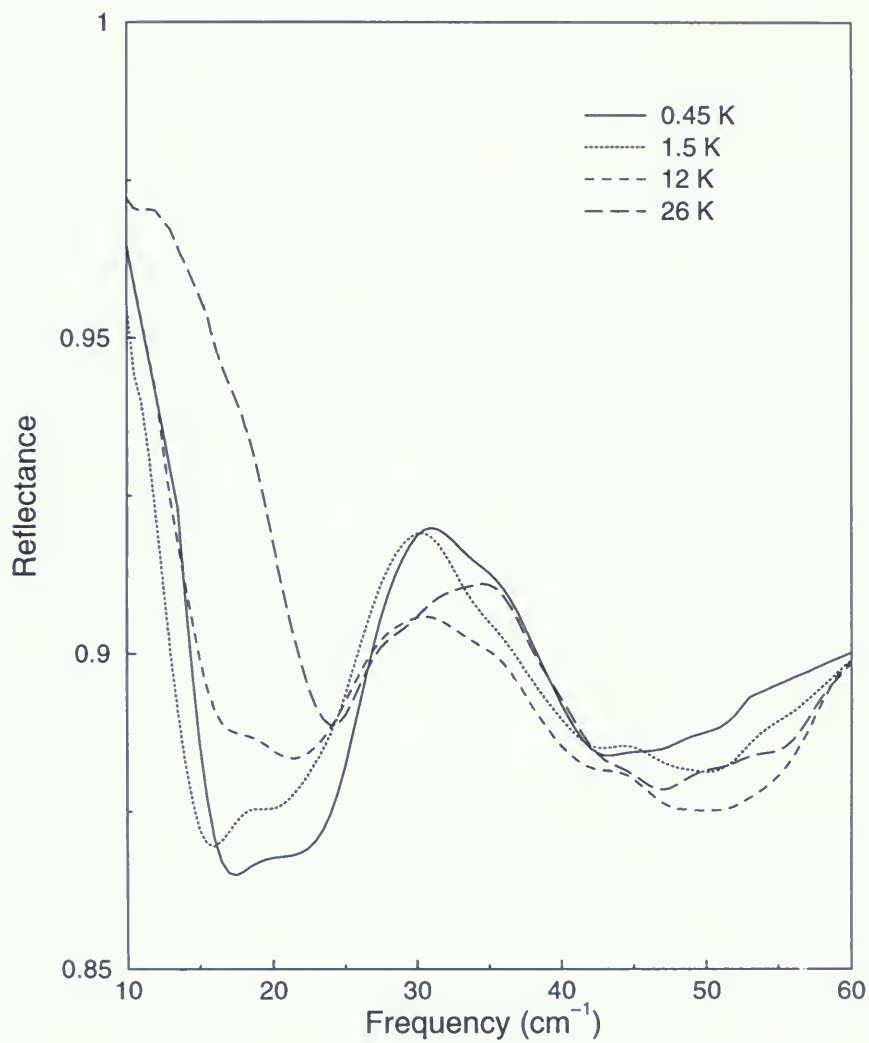


Figure 3.3: $(\text{TMTSF})_2\text{ClO}_4$ reflectance along the a -axis, for the slowly cooled sample.

superconducting critical temperature, T_c , which for this compound is 1.2 K. The raw data were interpolated and the graphs smoothed for clarity.

Chapter 4

Data Analysis: Thermorefectance and Optical Conductivity

4.1 Thermorefectance Below Anion-Ordering Temperature

Because the fast cooling data show no clear change with temperature below 26 K, we decided to calculate the thermorefectance of the other three data sets relative to the 26 K one, and indeed, the graphs obtained are flat curves, very close to the value 1. Thermorefectance is defined as the ratio of two reflectance data sets taken for the sample under the same conditions at different temperatures. The results are shown in Figure 4.1. For the slowly cooled sample, however, thermorefectance has considerable structure, indicating that the reflectance below 26 K is temperature dependent, more so at low frequencies, as one can see from the three pairs of curves presented, for comparison, on the same graph.

The temperature independence of the fast cooling case is in agreement with the results of Vescoli *et al.* [35], who found that there was no signature of the spin density wave gap parallel to the stacks in quenched samples.

4.2 Optical Conductivity

To see how the temperature dependence of the slow cooled sample data translates into optical conductivity, the Kramers-Kronig technique was applied to the reflectance data.

In order to use the Kramers-Kronig relations (see Appendix A) to obtain the complex optical conductivity $\sigma(\omega)$, one has to extrapolate the experimental data to cover the entire

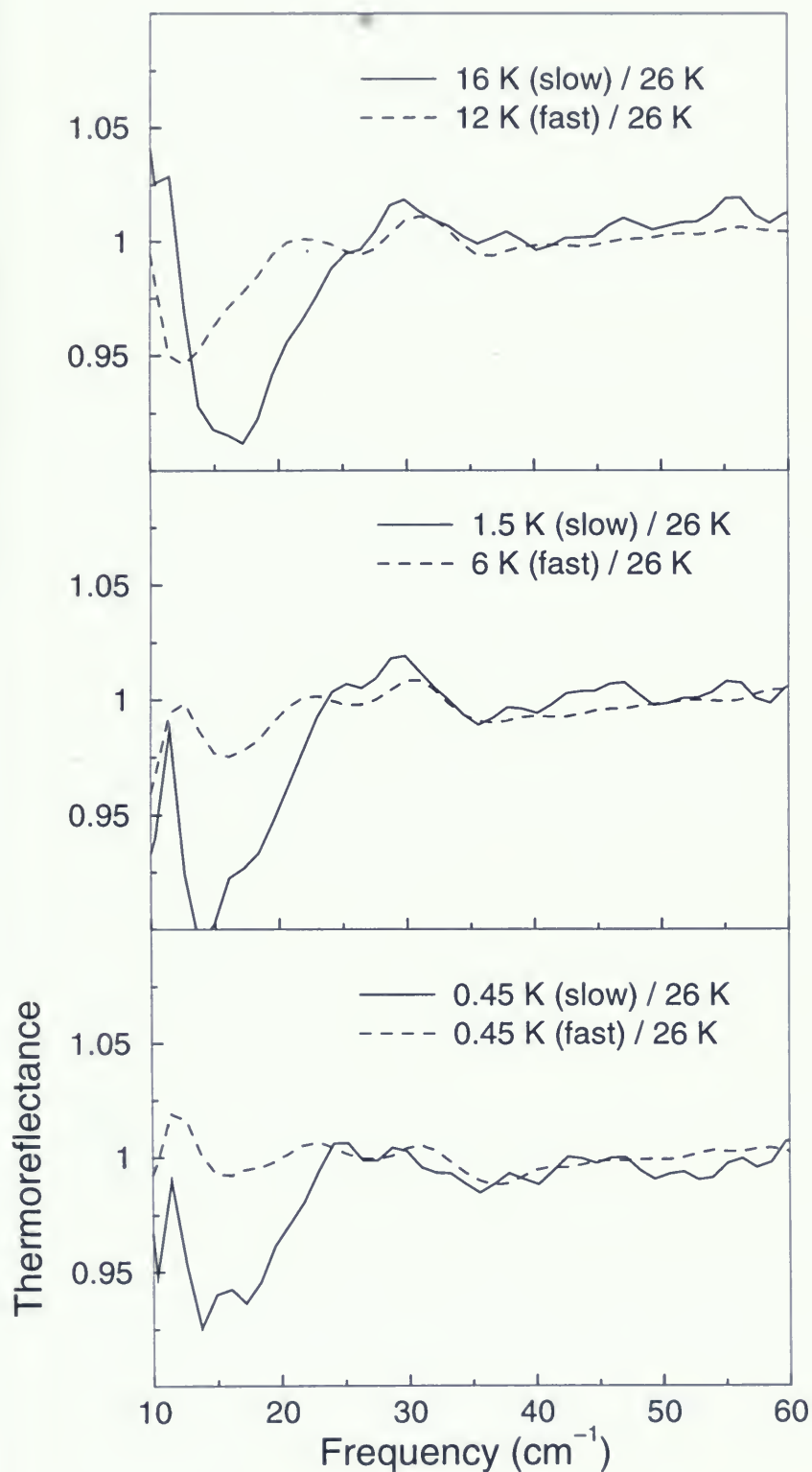


Figure 4.1: Thermorefectance (relative to 26 K) for the slow and fast cooling of the sample, with light polarized along the a -axis.

range of frequencies. Fortunately we could use reflectance results reported earlier for the same compound: for the 60 to 1000 cm^{-1} range by Cao and Timusk [2], and for the 1000 to 8000 cm^{-1} range by Kikuchi *et al.* [3]. Our data were extrapolated to zero frequency either by using a line extension to 1, or by using the Hagen-Rubens value [45], or by using the low frequency phonon reported by N. Cao and T. Timusk [2] (see, for example, the 26 K curves in Figure 4.2). The Hagen-Rubens reflectance value:

$$R(\omega) = 1 - \sqrt{\frac{2\omega}{\pi\sigma_{dc}}} \quad (4.1)$$

was determined for each temperature using the resistivity values reported by K. Bechgaard *et al.* [12]. We observe that these approximations do not seem to have significant influence on the Kramers-Kronig derived real conductivity $\sigma_1(\omega)$, in the range of our measurements (15 to 60 cm^{-1}), as can be seen in Figure 4.3.

Using the phonon from the data of Cao and Timusk causes the conductivity above approximately 20 cm^{-1} to shift down slightly, but does not change the shape of the broad band. The relative temperature dependence maintains the same trend for the different low frequency extrapolations.

Curves for the real part of the optical conductivity obtained from the reflectance data of Figure 3.3 by the Kramers-Kronig procedure (see Appendix A) are presented in Figure 4.4, for the slow cooling of the sample. We indicated the difference between the Hagen-Rubens (used here) and phonon low frequency extrapolations by vertical line segments originating on each curve.

The peak seen at approximately 35 cm^{-1} is asymmetric and grows with lowering the temperature, while the background low frequency conductivity seems to be losing spectral weight with decreasing temperature. Since we have no data below 10 cm^{-1} , we can presume that the spectral weight perhaps goes into a narrow peak at even lower frequencies.

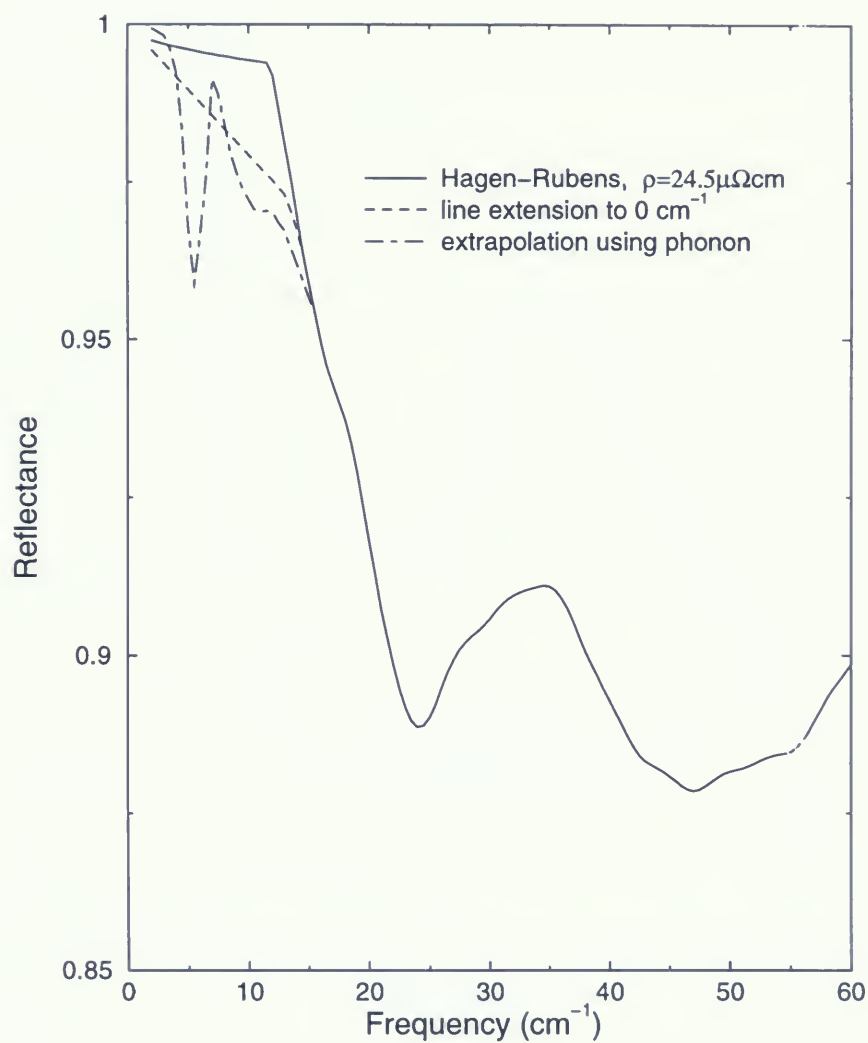


Figure 4.2: Reflectance at 26 K for the slow cooling of the sample, with light polarized along the a -axis, using three different low frequency extrapolations.

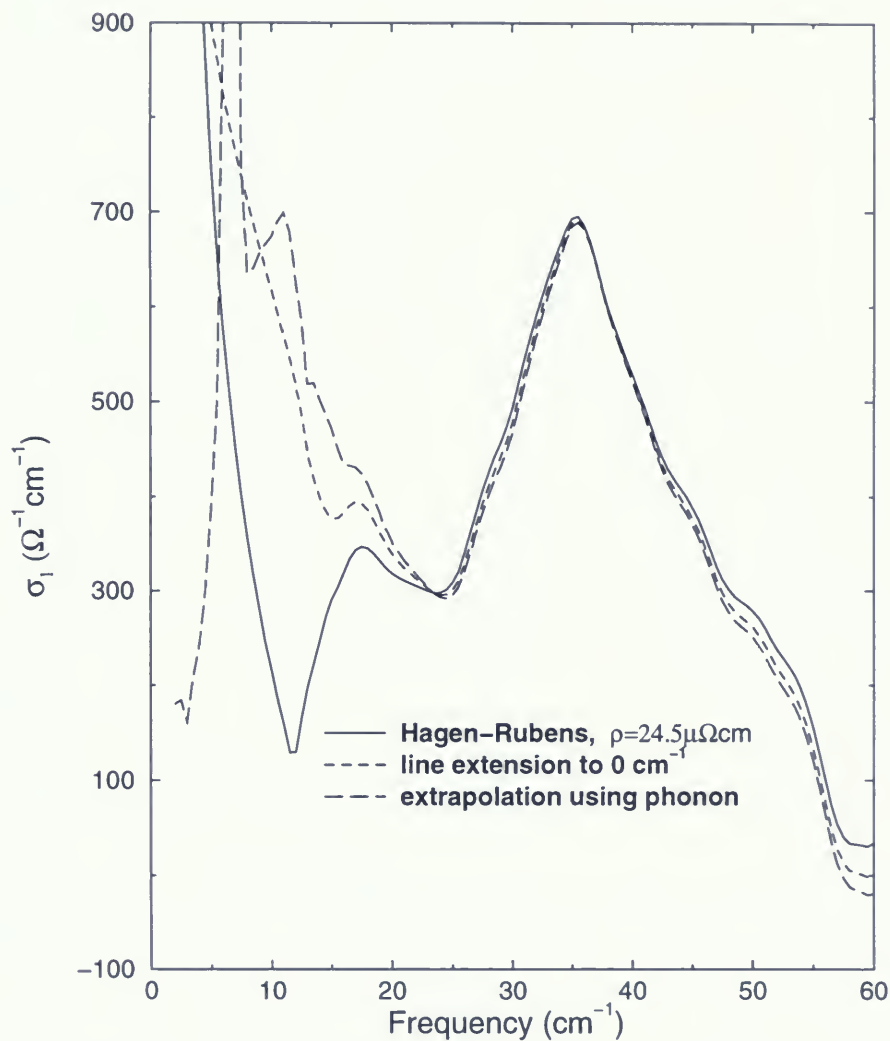


Figure 4.3: Real part of the optical conductivity for the slow cooling of the sample, at 26 K, with light polarized along the a -axis, derived from the three different low frequency extrapolations for reflectance.

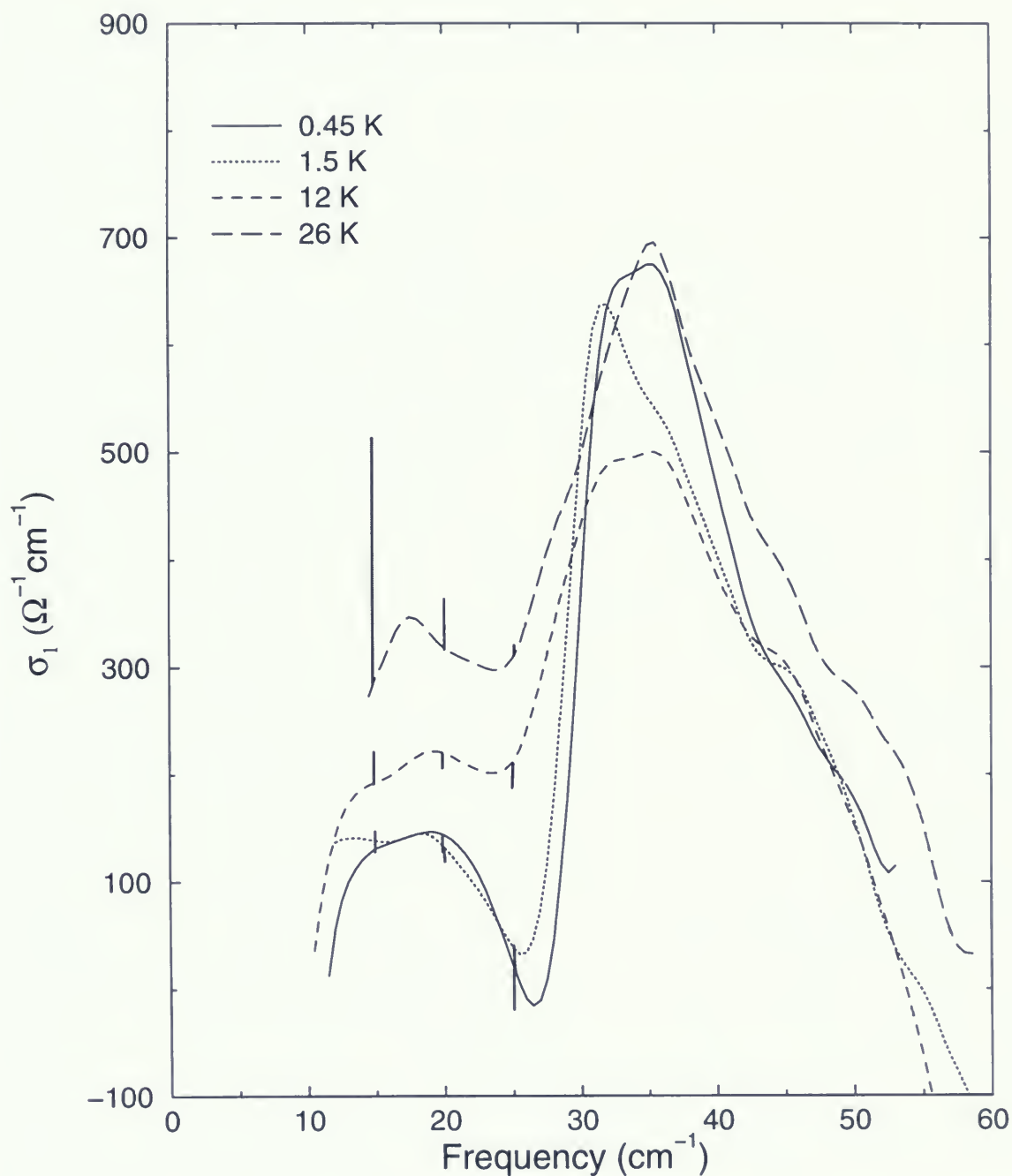


Figure 4.4: $(\text{TMTSF})_2\text{ClO}_4$ real part of the optical conductivity along a -axis, for the slow cooling of the sample. Line segments indicate the magnitude of the difference due to low frequency extrapolations, at 15, 20 and 25 cm^{-1} .

It should be noted that two peaks have been reported, at 7 cm^{-1} and 25 cm^{-1} , in the real part of the optical conductivity, along the a -axis, at temperatures down to 2 K [46].

Chapter 5

Discussion of Results and Conclusions

5.1 Results Discussion

Various measurements on $(\text{TMTSF})_2\text{ClO}_4$ at temperatures above the superconducting transition temperature have been interpreted [47] (in 1982) from the view point of the theory of fluctuational superconductivity to suggest the existence of a pseudogap of approximately 3.8 meV at low temperatures, and that superconducting fluctuations would exist at temperatures as high as 40 K.

Extensive far infrared measurements followed, in search for evidence of a superconducting pseudogap [1, 46]. These results supported the conclusion of Challener *et al.* [34] that there is no evidence for fluctuational superconductivity.

Further study of the feature in the reflectance near 30 cm^{-1} , as a function of temperature and applied magnetic field [1], indicated that this feature is caused by a sharp peak in the real part of the optical conductivity, as is expected for a coupled electron-phonon mode, rather than a gradual rise, as might be expected for a pseudogap. The feature's strong temperature dependence at the anion ordering transition indicates that it is associated with the ordering of the anions.

The absence of a magnetic field dependence at temperatures above the spin density wave transition (6 K), but well within the temperature range at which superconducting fluctuations were hypothesized to exist, argued against interpretation in terms of a pseudogap [1].

It is also known for $(\text{TMTSF})_2\text{ClO}_4$ that the Kramers-Kronig derived optical conductivity in the far infrared contrasts clearly with the high dc-conductivity, more so at low temperatures, in the a -axis direction [2, 12].

From Figure 3.3 one can see that the reflectance edge near 10 cm^{-1} exhibits a strong temperature dependence, and should be electronic in origin. This edge becomes sharper and deeper as the temperature decreases.

As can be estimated from the detail shown in Figure 5.1, on entering superconducting state this edge appears to shift up in frequency by approximately 2 cm^{-1} .

The peak near 30 cm^{-1} (reported as the ' 28 cm^{-1} feature' in Reference [1]) also shows a strong temperature dependence, as its intensity grows with decreasing temperature. If the mode represents an electron-phonon coupled mode then it should be sensitive to changes in electronic background. Therefore, if the electronic background has a shift, for example, due to the superconducting gap, the mode may also have a frequency shift. Upon entering the superconducting state the peak is also observed to shift to higher frequency, by approximately 2 cm^{-1} , as can be seen in Figure 5.2.

Indeed, the size of the shift in spectra from normal to superconducting state is consistent with calculations made using the BSC value of 3.53 for $\frac{2\Delta_0}{k_B T_c}$:

$$2\Delta_0 = 3.53k_B T_c = 3.53 \times 0.086 \frac{\text{meV}}{\text{K}} 1 \text{ K} = 2.45 \text{ cm}^{-1} \quad (5.1)$$

Further evidence that this mode is sensitive to the change in the electronic background (*i.e.* to going into the superconducting state) comes from comparing with its temperature dependence upon fast-cooling. As can be seen in Figure 5.2, the reflectance peak near 30 cm^{-1} in the fast cooling case is smaller than the corresponding peak seen in the slow cooling case, and does not show strong temperature dependence.

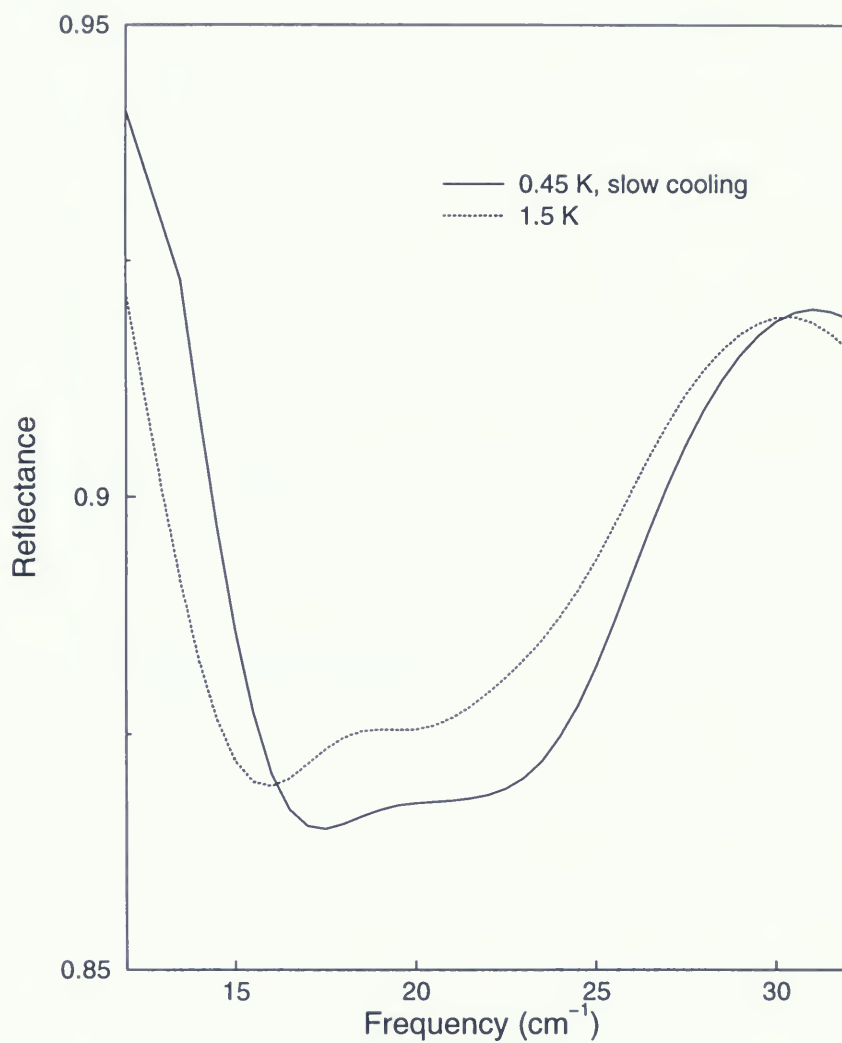


Figure 5.1: $(\text{TMTSF})_2\text{ClO}_4$ reflectance, along the a -axis, for the slowly cooled sample. Notice the shift to higher frequency in the low frequency edge, on going from 1.5 K to 0.45 K.

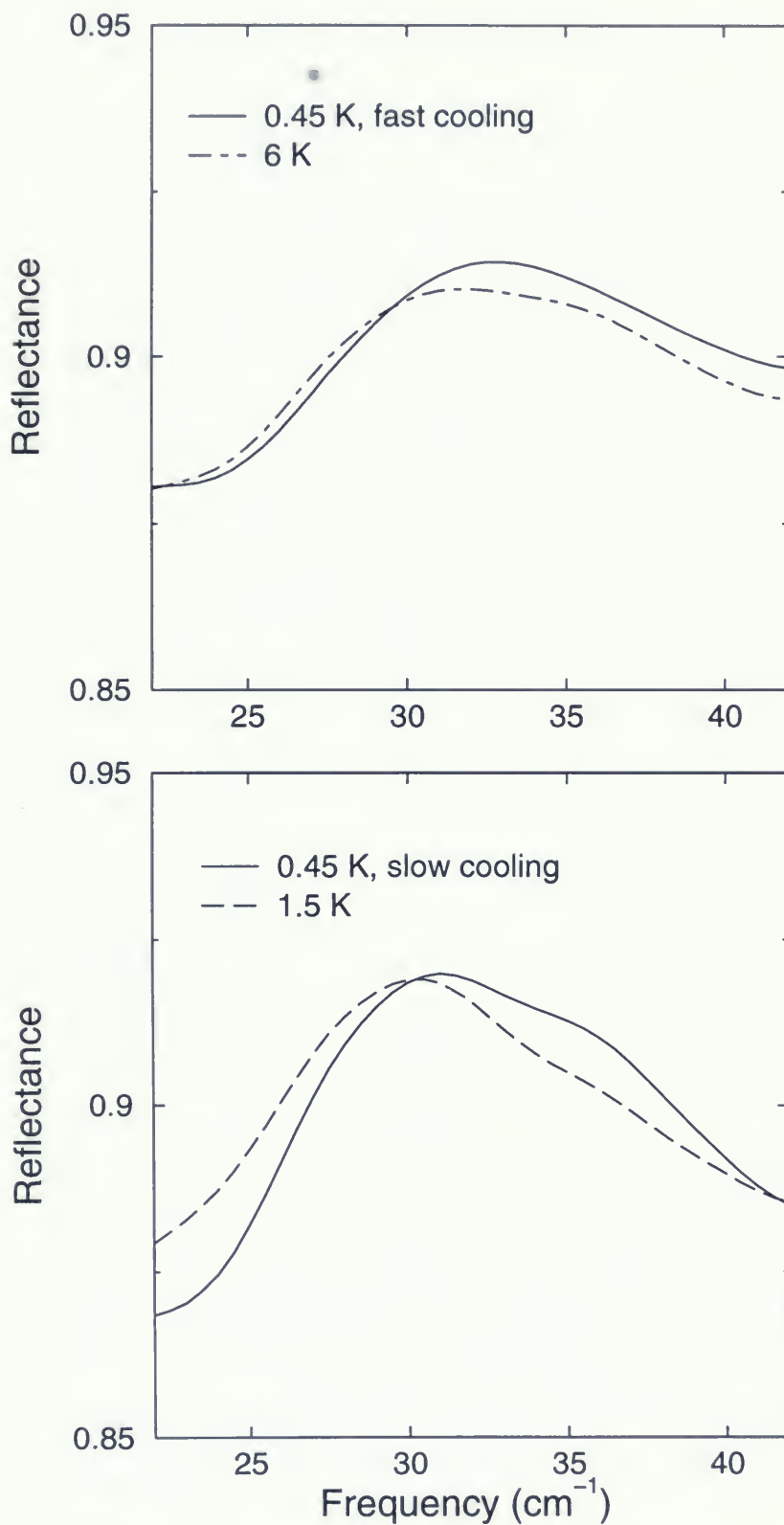


Figure 5.2: The 30 cm^{-1} peak in reflectance along the a -axis, for the fast and the slowly cooled sample, below and above the superconducting temperature of 1.2 K.

5.2 Conclusions

The experiments presented in this thesis explore, for the first time, the superconducting state of $(\text{TMTSF})_2\text{ClO}_4$ (and the transition from the normal to the superconducting state), in the far infrared region, from the perspective of optical spectroscopy.

The superconducting state of $(\text{TMTSF})_2\text{ClO}_4$ has been subject to very few studies, likely because of the low T_c and the fragility of the needle-like sample crystals. Neither the mechanism driving the superconducting instability, nor the symmetry of the superconducting order parameter have been established. The magnitude of the specific heat jump [26] and the energy gap deduced from tunneling spectroscopy [48] are consistent with conventional BCS theory. Using the technique of nuclear spin relaxation Takigawa *et al.* [49] inferred an anisotropic order parameter vanishing along lines on the Fermi surface. Belin and Behnia however carried out thermal conductivity measurements [50] and found that their results provide support for a nodeless superconducting gap function. They argued that the T^3 temperature dependence Takigawa *et al.* measured for the proton spin relaxation rate was limited to temperatures greater than $T_c/2$, and should not be taken as evidence for nodes in the gap function, because even for conventional BCS superconductors such exponential behaviour is expected only at very low temperatures. Belin and Behnia rule out nodes in the gap function, but leave open the possibility of an antisymmetric order parameter.

Our study reports the far infrared a -axis optical properties of $(\text{TMTSF})_2\text{ClO}_4$. We cannot determine the magnitude of the superconducting energy gap because, according to the tunneling and specific heat measurements, it is found to have a typical BCS value and would therefore appear at frequencies lower than those accessible, nor contribute to the knowledge of the gap structure, since the optical technique probes an average over the k -space.

We do however find evidence of strong electron-phonon coupling, which might indicate a conventional pairing mechanism, a fact that is in agreement with the conclusions of previous studies [1, 25].

Early measurements (1982) of the specific heat, magnetic critical field, and Meissner effect in the Bechgaard salts were all consistent with a conventional BSC theory in an anisotropic 3-D superconductor with a T_c of approximately 1 K [25]. The size of the experimentally observed shift of the low frequency reflectance edge and the 30 cm^{-1} peak in going from the normal to the superconducting state, presented here, supports that interpretation.

The peak near 30 cm^{-1} has been identified in earlier work as a coupled electron-phonon mode [46, 1]. There is some uncertainty regarding the nature of the rising low frequency reflectance. We deduce from the strong sharpening of this feature in this narrow temperature range that it is highly sensitive to the electronic structure. Ng *et al.* [46] and Challener *et al.* [34] have identified it as a sharp phonon mode at 7 cm^{-1} , while the measurements of Eldridge and Bates [51] do not resolve a phonon-like peak, the absence of which, they suggest could be the result of thermal cycling. We assumed that the reflectance continues smoothly to unity below 10 cm^{-1} (Hagen-Rubens extrapolation), in order to carry out a Kramers-Kronig analysis to obtain the optical conductivity.

The temperature and frequency dependence of the real part of the optical conductivity is not that expected for a simple metal, but rather reflects the removal at low temperatures of some electronic states at the Fermi level. As the temperature is lowered the low frequency background optical conductivity decreases in magnitude, while the 30 cm^{-1} mode becomes more asymmetric and gains oscillator strength. The sensitivity of the above mentioned mode to these changes in electronic structure supports its assignment as a strongly coupled electron-phonon mode.

Appendix A

Kramers-Kronig Analysis

Reflectivity and Phase Shift Dispersion Relations

Dispersion relations are prevalent throughout physics and derive from the causal nature of the response of materials, bodies or particles to electromagnetic, elastic or other fields. Kramers-Kronig relations [52, 53] are dispersion relations, *i.e.* integral formulae relating dispersive processes to absorption ones [54]. The classic example is the Kramers-Kronig relation that couples the real and imaginary parts of the complex dielectric function of a material:

$$\epsilon_1(\omega) - 1 = \frac{1}{\pi} \wp \int_{-\infty}^{\infty} \frac{\epsilon_2(\omega')}{\omega' - \omega} d\omega' = \frac{2}{\pi} \wp \int_0^{\infty} \frac{\omega' \epsilon_2(\omega')}{\omega'^2 - \omega^2} d\omega', \quad (\text{A.1})$$

where \wp denotes the principal value of the integral, and the last identity follows from the fact that

$$\epsilon_2(-\omega') = -\epsilon_2(\omega'). \quad (\text{A.2})$$

Similarly, we can write:

$$\epsilon_2(\omega) = -\frac{1}{\pi} \wp \int_{-\infty}^{\infty} \frac{\epsilon_1(\omega') - 1}{\omega' - \omega} d\omega' = -\frac{2\omega}{\pi} \wp \int_0^{\infty} \frac{\epsilon_1(\omega') - 1}{\omega'^2 - \omega^2} d\omega', \quad (\text{A.3})$$

with the condition that

$$\epsilon_1(-\omega') = -\epsilon_1(\omega'). \quad (\text{A.4})$$

The reflectivity (or reflectance) for a plane wave normally incident from vacuum on a medium with dielectric constant ϵ is defined as the fraction R of power reflected:

$$R = \frac{(E^r)^2}{(E^i)^2} = \frac{(1 - n)^2 + k^2}{(1 + n)^2 + k^2} \quad (\text{A.5})$$

where n and k are the real and imaginary parts of the complex refractive index,

$$n + ik = N. \quad (\text{A.6})$$

Defining the complex dielectric function and conductivity to be respectively:

$$\epsilon = \epsilon_1 + i\epsilon_2 = N^2 \quad (\text{A.7})$$

and

$$\sigma = \sigma_1 + i\sigma_2, \quad (\text{A.8})$$

one obtains:

$$\epsilon_1 = n^2 + k^2 \quad (\text{A.9})$$

and

$$\epsilon_2 = 2nk. \quad (\text{A.10})$$

But

$$\epsilon_2 = \frac{4\pi\sigma_1}{\omega}, \quad (\text{A.11})$$

where σ_1 denotes the real part of the optical conductivity [55].

The optical properties of interest are N , ϵ and σ . Knowing either N or ϵ yields the other and σ_1 , but it is obvious that one cannot obtain both n and k from the measured reflectivity R .

It is necessary to make use of the dispersion relations, in order to determine the optical properties or constants, if one measures a material's reflectivity at normal incidence.

The measured quantity $R(\omega)$ is related to the complex reflectivity amplitude r (the complex ratio of outgoing to incoming electromagnetic fields) by:

$$R(\omega) = r(\omega)r^*(\omega). \quad (\text{A.12})$$

Writing the complex reflectivity amplitude as:

$$r(\omega) = \rho(\omega)e^{i\theta(\omega)}, \quad (\text{A.13})$$

where $\rho(\omega)$ and $\theta(\omega)$ are the reflectivity coefficient and the phase shift due to reflection, respectively, equations A.5, A.12, and A.13 can be solved and n and k obtained in terms of $R(\omega)$ and $\theta(\omega)$.

If we write equation A.13 as:

$$\ln r(\omega) = \ln \rho(\omega) + i\theta(\omega), \quad (\text{A.14})$$

and argue that the reflectance must obey causality [54], we have the dispersion relations:

$$\ln \rho(\omega) = \frac{1}{\pi} \wp \int_{-\infty}^{\infty} \frac{\theta(\omega')}{\omega' - \omega} d\omega' \quad (\text{A.15})$$

and

$$\theta(\omega) = -\frac{1}{\pi} \wp \int_{-\infty}^{\infty} \frac{\ln \rho(\omega')}{\omega' - \omega} d\omega'. \quad (\text{A.16})$$

Then, from the condition that the input and output be real:

$$r(-\omega) = r^*(\omega), \quad (\text{A.17})$$

one can write equation A.16 as an integral over positive frequencies:

$$\theta(\omega) = -\frac{2\omega}{\pi} \wp \int_0^\infty \frac{\ln \rho(\omega')}{\omega'^2 - \omega^2} d\omega'. \quad (\text{A.18})$$

Further, if the principal value is eliminated (by subtracting an integral that is identically equal to zero), equation A.18 becomes:

$$\theta(\omega) = -\frac{2\omega}{\pi} \int_0^\infty \frac{\ln \rho(\omega') - \ln \rho(\omega)}{\omega'^2 - \omega^2} d\omega'. \quad (\text{A.19})$$

The integration of equation A.19 must be done numerically. Since $R(\omega)$ is determined experimentally only for a finite range of positive frequencies, it is also necessary to have some means of extrapolating the data, for the limits of the integration. After $\theta(\omega)$ is determined, the optical constants n and k (from equations A.5, A.12, and A.13), and hence ϵ_1 , ϵ_2 , and σ_1 can be calculated.

Bibliography

- [1] W. A. Challener, P. L. Richards, and R. L. Greene. Far infrared measurements of $(\text{TMTSF})_2\text{ClO}_4$. *Solid State Communications*, 51:765–768, 1984.
- [2] N. Cao, T. Timusk, and K. Bechgaard. Unconventional electrodynamic response of the quasi-one-dimensional organic conductor $(\text{TMTSF})_2\text{ClO}_4$. *Journal de Physique I (France)*, 6:1719–1726, 1996.
- [3] K. Kikuchi, I. Ikemoto, K. Yakushi, H. Kuroda, and K. Kobayashi. Temperature dependence of the reflectance spectrum of $(\text{TMTSF})_2\text{ClO}_4$. *Solid State Communications*, 42:433–436, 1982.
- [4] T. Ishiguro and K. Yamaji. *Organic Superconductors*. Springer-Verlag, Heidelberg, 1990.
- [5] N. Thorup, G. Rindorf, H. Soling, and K. Bechgaard. The structure of di-(2,3,6,7-tetramethyl -1,4,5,8-tetraselenafulvalenium) - hexafluorophosphate, $(\text{TMTSF})_2\text{PF}_6$, the first superconducting organic solid. *Acta Crystallographica*, B37:1236–1240, 1981.
- [6] H. Schwenk, K. Andres, and F. Wudl. Resistivity of the organic superconductor $(\text{TMTSF})_2\text{ClO}_4$ in its relaxed, quenched, and intermediate state. *Physical Review B*, 29:500–503, 1984.
- [7] A. Isihara. *Condensed Matter Physics*. Oxford University Press, Oxford, 1991.

- [8] M. Hildebrand. The infrared optical properties of Sr_2RuO and SmTiO , including an object-oriented resistivity interface. Master's thesis, Brock University, 1999.
- [9] Infrared Laboratories. *Brock University Instruction Manual*. 1994.
- [10] W. A. Little. Possibility of synthesizing an organic superconductor. *Physical Review*, 134:A 1416–1424, 1964.
- [11] K. Bechgaard, C. S. Jacobsen, K. Mortensen, and H. J. Pedersen. The properties of the highly conducting salts, $(\text{TMTSF})_2\text{X}$, where X is PF_6^- , AsF_6^- , SbF_6^- , BF_6^- or NO_3^- , derived from (TMTSF). *Solid State Communications*, 33:1119–1125, 1980.
- [12] K. Bechgaard, K. Carneiro, M. Olsen, F. B. Ramussen, and C. S. Jacobsen. Zero pressure organic superconductor: $(\text{TMTSF})_2\text{ClO}_4$. *Physical Review Letters*, 46:852–855, 1981.
- [13] S. S. P. Parkin, E. M. Engler, R. R. Schumaker, R. Lagier, V. Y. Lee, J. C. Scott, and L. Greene. Superconductivity in a new family of organic conductors. *Physical Review Letters*, 50:270–273, 1982.
- [14] C. Agosta. Introduction to organic metals. *Clark University web page*, 1996.
- [15] W. Krätschmer, L. D. Lamb, K. Fostiropoulos, and D. R. Huffman. Solid C_{60} : a new form of carbon. *Nature (London)*, 347:354–358, 1990.
- [16] R. J. Cava, H. Takagi, H. W. Zandbergen, J. J. Krajewski, W. F. Peck Jr., T. Siegrist, B. Batlogg, R. B. van Dover, R. J. Felder, K. Mizuhashi, J. O. Lee, H. Eisaki, and S. Uchida. Superconductivity in the quaternary intermetallic compounds $\text{LnNi}_2\text{B}_2\text{C}$. *Nature (London)*, 367:252–253, 1994.
- [17] M. Crişan. *Theory of Superconductivity*. World Scientific, Singapore, 1989.

- [18] T. Timusk. Infrared properties of exotic superconductors. *Physica C*, 317–318:18–29, 1999.
- [19] C. Bourbonnais and D. Jérôme. Electronic confinement in organic metals. *Science*, 281:1155–1156, 1998.
- [20] C. S. Jacobsen, D. B. Tanner, and K. Bechgaard. Optical and infrared properties of $(\text{TMTSF})_2\text{X}$ and $(\text{TMTTF})_2\text{X}$ compounds. *Physical Review B*, 28:7019–7032, 1983.
- [21] P. M. Grant. Electronic structure of the 2:1 charge transfer salts of TMTCF ($\text{C} = \text{S}, \text{Se}, \text{Te}$). *Journal de Physique, Colloque C3*, 44:C3–847–857, 1983.
- [22] N. Kinoshita, M. Tokumoto, H. Anzai, T. Ishiguro, G. Saito, T. Yamabe, and H. Teramae. ESR g factors of isolated $(\text{TMTSF})^+$ and $(\text{TMTSF})_2\text{ClO}_4$ single crystals: comparison with molecular orbital calculations. *Journal of the Physical Society of Japan*, 53:1504–1512, 1984.
- [23] P. C. Stein, P. Bernier, and C. Lenoir. High resolution NMR investigation in the organic conductors $(\text{TMTSF})_2\text{X}$, $\text{X} = \text{ClO}_4, \text{ReO}_4$. *Physica B*, 143:491–493, 1986.
- [24] L. Forró, K. Biliaković, J. R. Cooper, and K. Bechgaard. Magnetoresistance of the organic superconductor $(\text{TMTSF})_2\text{ClO}_4$: Kohler’s rule. *Physical Review B*, 29:2839–2842, 1984.
- [25] R. L. Green and P. M. Chaikin. Organic superconductors. *Physica B*, 126:431–440, 1984.
- [26] P. Garoche, R. Brusetti, D. Jérôme, and K. Bechgaard. Specific heat measurements of organic superconductivity in $(\text{TMTSF})_2\text{ClO}_4$. *Journal de Physique. Lettres*, 43:L147–L152, 1982.

- [27] B. P. Gorshunov, G. V. Kozlov, A. A. Volkov, V. Železný, and J. Petzelt. Dielectric function of TTF-TCNQ in the submillimetre range. *Solid State Communications*, 60:681–687, 1986.
- [28] M. Dressel, A. Schwartz, G. Grüner, and L. Degiorgi. Deviations from drude response in low-dimensional metals: Electrodynamics of the metallic state of $(\text{TMTSF})_2\text{PF}_6$. *Physical Review Letters*, 77:398–401, 1996.
- [29] D. B. Tanner, C. S. Jacobsen, A. F. Garito, and A. J. Heeger. Infrared conductivity of (TTF-TCNQ) films. *Physical Review Letters*, 32:1301–1305, 1974.
- [30] P. Pouget, G. Shirane, K. Bechgaard, and J. M. Fabre. X-ray evidence of a structural phase transition in $(\text{TMTSF})_2\text{ClO}_4$, pristine and slightly doped. *Physical Review B*, 27:5203–5206, 1983.
- [31] C. Kittel. *Introduction to Solid State Physics*. John Wiley & Sons, New York, 7th edition, 1996.
- [32] F. Pesty, P. Garoche, and K. Bechgaard. Cascade of field-induced phase transitions in the organic metal $(\text{TMTSF})_2\text{ClO}_4$. *Physical Review Letters*, 55:2495–2498, 1985.
- [33] H. K. Ng, T. Timusk, and K. Bechgaard. Far-infrared properties of $(\text{TMTSF})_2\text{ClO}_4$ at low temperatures. *Journal de Physique, Colloque C3, supplément au n° 6*, 44:C3–867–872, 1983.
- [34] W. A. Challener, P. L. Richards, and R. L. Greene. Far infrared properties of $(\text{TMTSF})_2\text{ClO}_4$. *Journal de Physique, Colloque C3, supplément au n° 6*, 44:C3–873–878, 1983.
- [35] V. Vescoli, L. Degiorgi, B. Alavi, and G. Grüner. The spin-density wave gap in $(\text{TMTSF})_2\text{ClO}_4$. *Physica B*, 244:121–124, 1998.

- [36] V. Vescoli, L. Degiorgi, W. Henderson, G. Gruner, K. P. Starkey, and L. K. Montgomery. Dimensionality-driven insulator-to-metal transition in the bechgaard salts. *Science*, 281:1181–1184, 1998.
- [37] H. Basista, D. A. Bonn, T. Timusk, J. Voit, D. Jérôme, and K. Bechgaard. Far infrared optical properties of (TTF-TCNQ). *Physical Review B*, 42:4088–4099, 1990.
- [38] M. J. Rice. Organic linear conductors as systems for the study of electron-phonon interactions in the organic solid state. *Physical Review Letters*, 37:36–39, 1976.
- [39] M. J. Rice, L. Pietronero, and P. Bruesch. Phase phonons and intramolecular electron-phonon coupling in the organic linear chain semiconductor TEA(TCQN)₂. *Solid State Communications*, 21:757–760, 1977.
- [40] P. A. Lee, T. M. Rice, and P. W. Anderson. Fluctuation effects at a Peierls transition. *Physical Review Letters*, 31:462–465, 1973.
- [41] P. A. Lee, T. M. Rice, and P. W. Anderson. Conductivity from charge or spin density waves. *Solid State Communications*, 14:703–709, 1974.
- [42] D. B. Romero, C. D. Porter, D. B. Tanner, L. Forró, D. Mandrus, L. Mihaly, G. L. Garr, and G. P. Williams. Quasiparticle damping in Bi₂Sr₂CaCu₂O₈ and Bi₂Sr₂CuO₆. *Physical Review Letters*, 68:1590–1593, 1992.
- [43] C. C. Homes, M. Reedyk, D. A. Cradles, and T. Timusk. Technique for measuring the reflectance of irregular, submillimeter-sized samples. *Applied Optics*, 32, no.16:2976–2983, 1993.
- [44] H. Anzai, S. Maki, S. Takasaki, S. Tanaka, S. Nakatsuji, J. Yamada, K. Nozaki, A. Negishi, and M. Harusawa. Effect of electrode-materials for electrocrystallization

- of organic charge transfer complex $(\text{TMTSF})_2\text{ClO}_4$. *Journal of Crystal Growth*, 191:148–152, 1998.
- [45] J. M. Ziman. *Principles of the Theory of Solids*. Cambridge University Press, Cambridge, England, 2nd edition, 1972.
- [46] H. K. Ng, T. Timusk, J. M. Delrieu, D. Jérôme, K. Bechgaard, and J. M. Fabre. Observation of a gap in the far-infrared magneto-absorption of $(\text{TMTSF})_2\text{ClO}_4$: possibility of one-dimensional fluctuating superconductivity. *Journal de Physique. Lettres*, 43:L-513–L-519, 1982.
- [47] D. Jérôme and H. J. Schultz. Organic superconductors. *Advances in Physics*, 43:443–526, 1982.
- [48] H. Bando, K. Kajimura, H. Anzai, T. Ishiguro, and G. Saito. superconducting tunneling in $(\text{TMTSF})_2\text{ClO}_4/\text{a-Si/Pb}$ junctions. *Molecular Crystals and Liquid Crystals*, 119:41–44, 1985.
- [49] M. Takigawa, H. Yasuoka, and G. Saito. Proton spin relaxation in the superconducting state of $(\text{TMTSF})_2\text{ClO}_4$. *Journal of the Physical Society of Japan*, 56, no.3:873–876, 1987.
- [50] S. Belin and K. Behnia. Thermal conductivity of superconducting $(\text{TMTSF})_2\text{ClO}_4$: evidence for a nodeless gap. *Physical Review Letters*, 79, no.11:2125–2128, 1997.
- [51] J. E. Eldridge and G. S. Bates. The far infrared properties of $(\text{TMTSF})_2\text{PF}_6$ and $(\text{TMTSF})_2\text{ClO}_4$ at 6 k. *Molecular Crystals and Liquid Crystals*, 119:183–190, 1985.
- [52] H. A. Kramers. *Nature*, 117:775, 1926.
- [53] R. de L. Kronig. *Journal of the Optical Society of America*, 12:547, 1926.

- [54] F. Wooten. *Optical Properties of Solids*. Academic Press, London, 1972.
- [55] N. W. Ashcroft and N. D. Mermin. *Solid State Physics*. Saunders College, Philadelphia, 1976.





